Volume 5, Issue 1, 2021 ISSN: 2617-3522
DOI: https://doi.org/10.31058/j.am.2021.51001

First Principles Investigation of the Structural, Mechanical and Thermodynamic Stability of New 18-Valence RhVSi Half-Heusler Semiconductor

Omosede. E. Osafile[1*], Judith. O. Umukoro[1]

[1] Department of Physics, Federal University of Petroleum Resources, Effurun, Nigeria

Email Address

osafile.omosede@fupre.edu.ng (O. E. Osafile)
*Correspondence: osafile.omosede@fupre.edu.ng

Received: 15 May 2021**; Accepted:** 17 June 2021**; Published:** 27 June 2021

Abstract:

We have investigated the structural, electronic, elastic, mechanical, thermodynamic, and phonon properties of RhVSi half Heusler alloy in this work. The alloy obeys the Slater-Pauling rule. It is a face-centered cubic C1b structure. It exhibits a lattice parameter of 5.71 eV and a narrow indirect bandgap of 0.285 eV, making it attractive as an absorber in solar systems. The alloys have 18-valence electrons, and they obey the Slater-Pauling rule. The negative formation energy of 0.33 shows that experimental simulation is possible; it also confirms the structure's stability. The elastic properties obey the stability criteria set by Born and Huang and are, therefore, stable. We analyzed the alloy's mechanical strength, and it proves to be a superhard material with a Vickers hardness of 60.266 GPa. The Debye temperature of 408.375 K shows that the compound is hard and possesses a large wave velocity (3421.230 m/s) and will have high thermal conductivity. From investigations on the phonon properties using a 4 x 4 x 4 supercell to facilitate convergence, there are no negative frequencies; hence, we submit that the RhVSi half Heusler semiconductor is dynamically stable and can be simulated experimentally.

Keywords:

Density Functional Theory, Density Functional Perturbation Theory, Half-Heusler Semiconductor, Lattice Dynamics, Thermodynamic Properties, Phonon Properties

1. Introduction

The oscillations atoms undergo in a solid crystal lattice about its equilibrium position is referred to as vibrations. These vibrations account for material properties such as electrical conductivity, thermal conductivity, specific heat, optical and dielectric properties. The continuous fluctuations which arise from the thermal energy are more pronounced with an increase in temperature. These lattice vibrations result in a motion that produces waves that travels within the area of vibration in the lattice,

and these waves are called phonons. The phonon properties of material influence its thermal, optical, and electronic properties. Phonons have a density of state, which is controlled by the dimensionality of the material.

The Heusler family of alloys [1] has contributed immensely to searching for materials with industrially viable phonon properties for optoelectronic devices. Since the discovery of Heusler alloys, some variants have emerged, ranging from the full, half [2], inverse, to quaternary Heusler alloys [3,4]. Of these variants, the half Heusler alloys have proven to be quite useful in technological applications [5,6,7,8,9]. They find applications in thermoelectric devices [10], giant magnetoresistance sensors (GMR) [11], spintronics [12], as topological insulators, among others. In general, a half Heusler alloy, XYZ, has a $C1_b$ structure. The half Heusler alloy structure is similar to a full-Heusler alloy (X_2YZ) structure, with the $L2_1$ structure, save for missing one X element. X and Y are transition-metal, and Z is a main group element. The $C1_b$ structure of the half Heusler RhVSi is shown in Fig. 1, and the nomenclature for atomic positions are credited to Wyckoff [13,14]. The structure is drawn from the NaCl rock-salt structure with atomic positions (0, 0, 0) and (0.5, 0.5, 0.5) and the zincblende structure with atomic positions (0, 0, 0) and (0.25, 0.25, 0.25).

Although much research has been done on half Heusler alloys, to our knowledge, reports from first-principles calculation and experimental reports searching for viable ternary half Heusler alloys predicted to be stable in literature leaves room for more work in this area. In response to this, using the Perdew-Burke-Ernzerhof (PBE) with the generalized gradient approximation (GGA) in the density functional theory, we carry out a hypothetical investigation of the structural, electronic, mechanical and phonon properties of the half Heusler RhVSi compound.

2. Computational Method

Using the quantum espresso code (QE) [15], we studied the structural, electronic, mechanical and phonon properties RhVSi half Heusler alloy from first principles. The potentials for calculations were constructed using the projector augmented wave (PAW) [16,17] method, and the generalized gradient approximation (GGA) was employed to treat the Perdew-Burke-Erzhenhof exchange and correlation between electrons [18]. The Monkhorst-Pack scheme [19] was used to construct an 8×8×8 grid for the electronic structure calculation, and the converged value of the kinetic energy cutoff of the plane-wave used as a basis function was 70 eV. For the alloy, we fully relaxed each component atom in the unit-cell using the Broyden–Fletcher–Goldfarb–Shanno (BFGS) to obtain the equilibrium configuration for the atomic positions. A much denser k-point mesh of (20×20×20) grid with a tetrahedra occupation was used in calculating the electronic density of states. The alloys' behaviour at equilibrium temperature in terms of the volume and pressure was calculated by fitting the result obtained from the total energy calculation to the Birch-Murnaghan equation of state [20,21,22]. We treated the compound as a ferromagnetic system in the fcc crystallized phase. We subjected the equilibrium kinetic energy cutoff and k-point mesh to a convergence test. We selected dense high symmetry k-points for the FCC structure using (X-window) Crystalline Structures and Densities (XCrySDen) package [23] for the band structure calculations. The mechanical properties were determined using the quasi-harmonic approximation coded in the thermo-pw package as a post-proc in QE, which explored Voigt, Reuss, and Hill's approximation. [24,25,26].

3. Results and Discussions

3.1 Structural Properties

The most stable crystal structure of RhVSi is shown in Figure 1. RhVSi crystallizes in the face-centred cubic structure in the space group $F\bar{4}3m$ and space number 216 as a non-magnetic semiconductor. The electronic configuration of the elements investigated is $3d^8 5s^1$ and $3d^3 4s^2$ for rhodium and vanadium, respectively, while Si is $3s^2\ 3p^2$. The alloys crystallize in the MgAgAs structure with X, Y, Z atoms occupying the atomic positions (0, 0, 0), (0.25, 0.25, 0.25) and (0.75, 0.75, 0.75) respectively. The equilibrium lattice parameter is 5.71. As expected, RhVSi obeys the Slater-Pauling rule for hH alloys, and it crystallizes as a non-magnetic semiconductor. We confirmed this by using the rule for 18 valence electrons $M_t = Z_t - 18$ as proposed by Slater & Pauling, where Z_t is the alloy's valence number, and M_t is the magnetic moment per unit formula of the alloy. In our case, Z_t is 18.

The volume optimized lattice parameter computed for RhVSi is in reasonable agreement with the value reported in the literature [27]. Considering that RhVSi is being investigated for the first time, there are no experimental nor theoretical data available to compare the results of other parameters presented in this work. Hence, the data presented here can act as a reference for future investigations.

The results obtained during lattice optimization for energy and volume is fitted to the Murnaghan equation of state using:

$$\Delta E(V) = E - E_0 = BV_0\left[\left(\frac{V_n}{B^{'}}\right) + \left(\frac{1}{1-B^{'}}\right) + \left(\frac{V_n}{B^{'}\left(B^{'}-1\right)}\right)\right]$$

Where E_0 and V_0 are equilibrium values of energy and volume, respectively, without the effect of pressure, while B and B denote the bulk modulus and its derivative, respectively, the relationship between the energy and volume is shown in Figure 2. The bulk modulus value, pressure derivative of bulk modulus, volume, ground state energy, formation energy, energy bandgap, and lattice constant using PBE-GGA are presented in Table 1. The compound's magnetic moments are found to be zero in all three interacting elements confirming its non-magnetic nature. Each alloy element's atomic mass is 102.9055 u, 50.9415 u, and 28.0855 u for Rh, V and Si, respectively, and a total atomic mass unit of 181.9325 u. The atomic mass and lattice always reflect the amount of energy required for the atoms' interaction, which is -731.03 Ry.

Table 1. *Lattice constant (a_0), ground state energy E, bulk modulus B_0, pressure derivative of the bulk modulus B_0', volume V_0, the formation energy ΔE_f, and energy bandgap (E_g) of RhVSi compound in the most stable state using PBE-GGA.*

Compound	***a_0 (Å)***	**E *(Ry)***	***B_0 (GPA)***	***B_0'***	***V_0 (a.u.)³***	***ΔE_f (Ry)***	E_g (eV)
RhVSi	5.71 5.69 [27]	-731.03	179.7	4.42	314.70	-0.33	0.2848

One test for ascertaining an alloy's structural stability and establishing the possibility of experimental simulation of the alloy is deduced using the compound's formation energy. Negative formation energy supports simulation, while positive formation energy prohibits experimental simulation. The formation energy is

calculated by subtracting each element's energy from the bulk energy using the equation; $E_{form} = \frac{1}{3}[E_0 - (E_X + E_Y + E_Z)]$. The formation energy obtained for RhVSi is -0.33 eV showing that the alloy is structurally stable, establishing the possibility of experimental simulation.

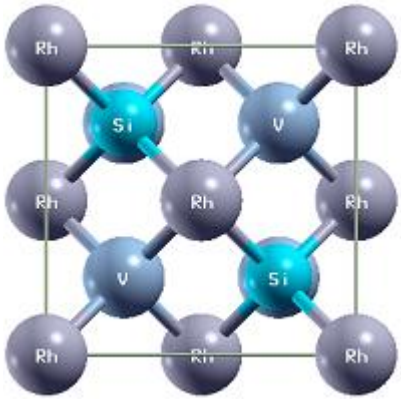

Figure 1. *The most stable crystal structure of RhVSi at the atomic positions (0, 0, 0), (0.25, 0.25, 0.25) and (0.75, 0.75, 0.75) for Rh, V, Si respectively.*

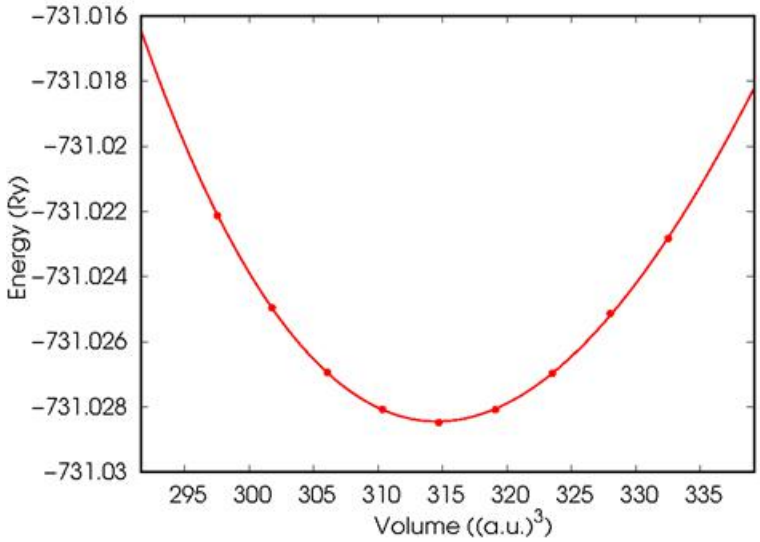

Figure 2. *Lattice optimization for the minimum energy versus volume as fitted to the Murnaghan equation of state.*

3.2. Electronic Properties

We present results for the electronic structure of the RhVSi compound, and the result presented includes the density of states (DOSs) and electronic band structure calculations using PBE-GGA. The FCC structure's band structure calculation is along the high symmetry path K→Γ→X→W→K→Γ→L with a dense k-point. From the band structure in Figure 3, sharper or steeper slopes are observed at the Γ point, the centre of the crystal momentum space or k = 0 space and X (the edge π/L of the first Brillouin zone in the 001 direction) symmetric point. The steep dispersion indicates a stronger orbital interaction arising from the d-orbitals of Rh and V, resulting in a possible increase in the mobility of charges. The steeper slope also suggests a covalent bonding between the d^8 orbital of Rh and d^3 orbital of V. Γ→X. the bandgap shows that Rh's d states are delocalized in the region of the Fermi energy. On the other hand, shallow or flat bands are observed between W→K symmetry points,

indicating ionicity and low group velocity resulting from the *s* and *p* orbitals' localization. The flat bands in the conduction band occur around 1 eV and 2 eV, while the flat bands are seen in the valence band around -1 eV to -3 eV.

Figure 3 shows the electronic band structure and states' electronic density for RhVSi alloy in the non-magnetic (paramagnetic) state. RhVSi exhibits an indirect bandgap of approximately 0.2848 eV between Γ and X high symmetry points. The conduction band minimum CBM is 14.2824 eV, while the valence band maximum is 13.9979 eV. The narrowness of the bandgap supports charge mobility. The density of states plot in Figure 3a shows that CBM is characterized by the 5*s* states of Rh, the 4s states of V, the 3s states of Si, on the other hand, the 3d and 3p states of Rh and Si dominate the VBM with degeneracies at gamma.

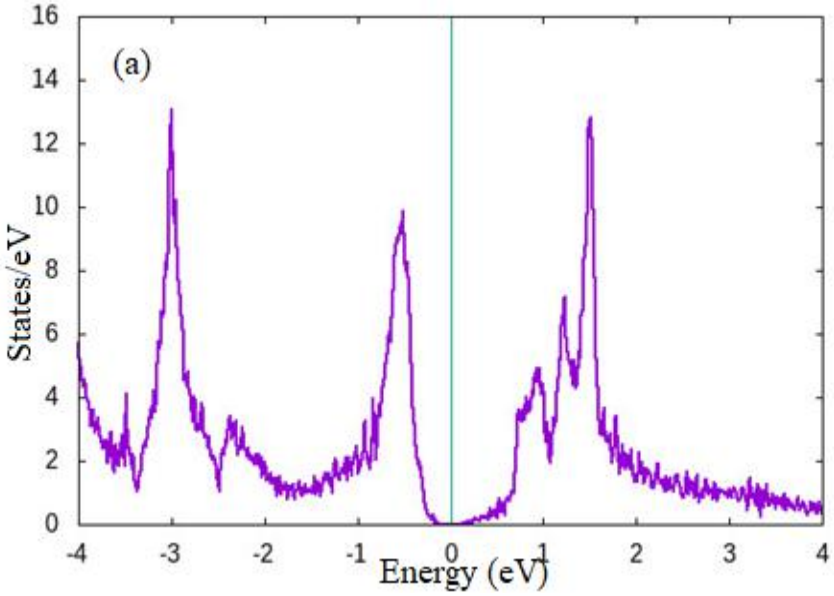

Figure 3 a. *Total electronic density of states of RhVSi half Heusler alloy using the DFT-GGA approximation.*

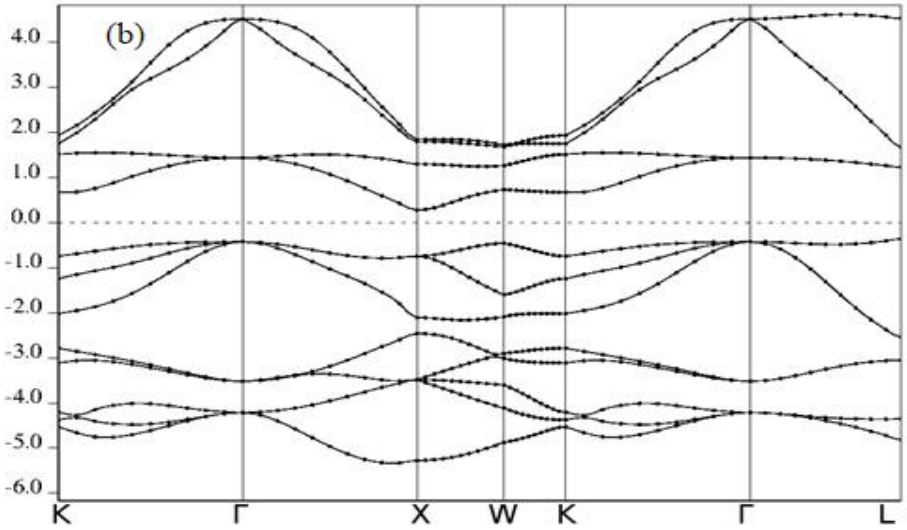

Figure 3b. *Band-structure calculation of RhVSi half Heusler alloy using the DFT-GGA approximation.*

3.3. Elastic Properties and Mechanical Stability

The aim of this investigation includes establishing the stability of RhVsi half Heusler semiconductor for possible technological application. Hence, in this section, we present results for the computation of the compound's elastic properties and mechanical stability. The computation was done using the linear response density functional perturbation theory as implemented in the thermo-pw code. Max Born and collaborator proposed the parameters and criteria required to predict the stability of a cubic compound. The parameters include fundamentally C_{11}, C_{12} & C_{44}. According to Born & Huang (1954) [28], the following conditions $C_{11} > 0; C_{44} > 0; \frac{1}{2}(C_{11} - C_{12}) > 0; \frac{1}{3}(C_{11} + 2C_{12}) > 0$, among others, must be satisfied for the compound to be described as stable. These conditions are called the Born stability criteria; also, we ensure the order $C_{11} > C_{12} > C_{44}$ is respected for the parameters (C_{11}, C_{12}, C_{44}). It is also required that $C_{12} < B < C_{11}$ where B is the bulk modulus. C_{11} describes the degree of stiffness of materials against principal strains, and C_{44} describes the stiffness of the bulk crystal structure and is a determinant of the resistance against shear deformation. From the results obtained and documented in Table 3, the alloy fulfils all conditions for stability. We give in Eqn. (1), another relation that further strengthens the assertions on the stability of materials. It states that a crystalline structure can also be classified as stable if, in the harmonic approximation, the elastic energy is a positive definite$(E > 0, \forall \varepsilon \neq 0)$ in the absence of external load [29].

$$E = E_0 + \frac{1}{2}V_0 \sum_{i,j=1}^{6} C_{i,j}\varepsilon_i\varepsilon_j + 0(\varepsilon^3) \quad (1)$$

This condition is termed the elastic stability criterion. It must satisfy the necessary and sufficient stability conditions that matrix C and C's eigenvalues are favourable. The results we present in Table 2 confirm that the alloy obeys all stability criteria and is stable.

Table 2. *Elastic properties in GPa of RhVSi half Heusler semiconductor using the density functional perturbation theory.*

Compound	$\mathbf{C_{11}}$	$\mathbf{C_{12}}$	$\mathbf{C_{44}}$	$\frac{1}{2}(\mathbf{C_{11} - C_{12}})$	$\frac{1}{3}(\mathbf{C_{11} + 2C_{12}})$
RhVSi	212.875	135.647	84.129	77.228	161.390

Other elastic and mechanical properties computed include bulk, shear, and Young's moduli. The moduli properties were computed using the following Equations.

$$B = \frac{1}{3}(C_{11} + 2C_{12}) \quad (2)$$

$$G = \frac{1}{2}(G_V + 2G_R) \quad (3)$$

$$E = \frac{9BG}{3B+G} \quad (4)$$

Where G_V and G_R in Eqn. (4) are the Voigt and Reuss approximations of the shear modulus, respectively, and are obtained using.

$$G_V = \frac{1}{5}(C_{11} - C_{12} + 3C_{44}) \quad (5)$$

$$G_R = 5\frac{(C_{11}-C_{12})C_{44}}{3(C_{11}-C_{12})+4C_{44}} \quad (6)$$

The bulk modulus B characterizes the ability of a material to resist fracture. Hence, it defines the hardness of the material, and the shear modulus G describes the resistance of the material to plastic deformations. The Young's modulus E, on the other hand, is the ratio of tensile stress to tensile strain, and it measures the stiffness of

the material. We derived the alloys' moduli using the Voigt and Reuss approximation directly from C_{11}, C_{12}, and C_{44}. A stiff material has a high Young's modulus, while a ductile material has a low young's modulus.

We also compute and present results in Table 3. for some mechanical characteristics including anisotropy, Poisson ratio, the Pugh's ratio (B/G) for ductility/brittleness, Cauchy's pressure, and Vicker's hardness using Eqns. (7-10)

$$A = \frac{2C_{44}}{C_{11}-C_{12}} \tag{7}$$

$$\upsilon = \frac{1}{2}\left(\frac{3B-2G}{3B+G}\right) \tag{8}$$

$$C^P = C_{12} - C_{44} \tag{9}$$

$$H_V = 0.92\left({}^{B}/_{G}\right)^{1.3137} G^{0.708} \tag{10}$$

A, υ, C^P, and H_V are the anisotropy factor, Poisson ratio, Cauchy pressure, and the Vicker's hardness. The Poisson ratio and the Cauchy pressure suggests the possible bonding of the atoms in the compound. Frantsevich et al. reported a critical value of 0.26 for the Poisson ratio [30]. This critical value separates between covalent bonding and ionic bonding; from the results in Table 4, the Poisson ratio favours ionic bonding in the compound. A sizeable negative C^P supports directional covalent bonding, while a positive value suggests non-directional metallic bonding. The compound's results are positive and substantial, hence, supporting a non-directional metallic bonding among the atoms. In isotropic materials, the material properties are independent of the direction, while the material properties are direction-dependent in anisotropic materials. When a material is measured from different directions, any deviation from unity automatically renders the material anisotropic. The values obtained for the anisotropy/isotropy test of the materials is 2.177; the result shows that RhVSi alloy is anisotropic. The anisotropy value also suggests a high susceptibility to cracking during experimental analysis because the more extensive the deviation from unity, the more susceptible it is to cracks during an experimental simulation.

Using the ratio of bulk modulus to the shear modulus (B/G) of a material, Pugh [31] establishes 1.75 as the critical value between brittleness and ductility in a material. When the B/G value is below/above the reference value, the material is brittle/ductile. The brittleness or ductility of a material can affect the failure mode in fabrication processes. The results in Table 3 predicts the material is ductile, with a Pugh ratio of 2.62. The Vicker's hardness holistically addresses the resistance of the material to indentation. Tian et al. predict that materials whose Vicker's hardness is above 40 GPa are superhard materials [32]. Our results show that RhVSi alloy is a superhard material. The Young's modulus of 163.736 GPa recorded for RhVSi alloy falls within the range of 169 GPa recorded for silicon wafer in the 001 direction [33]. Finally, all results for elastic and mechanical stability test leads to the prediction that the RhVSi alloy is mechanically stable at room temperature.

Table 3. *Computed values of Poisson ratio (v), bulk modulus (B in GPa), shear modulus (G in GPa), Pugh's ratio (B/G), Debye temperature (θ in K), anisotropy (A), Young's modulus (E in GPa), Vickers hardness (H_v in GPa), Cauchy pressure (C^P in GPa), and the density (ρ in g/cm^3) using the linear response density functional perturbation theory.*

Compound	ν	B	G	${}^{B}/_{G}$	θ	A	E	H_v	C^P	ρ
RhVSi	0.33	161.39	61.55	2.62	408.38	2.18	163.74	60.27	51.52	6.49

3.4. Thermodynamic Stability

Thermodynamic stability is critical in correctly recommending a material for any experimental procedure. In this section, we present results for specific vital thermodynamic processes. We carried out the calculations using the quasi-harmonic approximation (QHA) rather than the harmonic approximation. The harmonic approximation fails to account for thermal expansion and thermal transport as temperature increases and does not take phonon interactions into account; hence the phonon lifetime is interpreted as infinite. Effective implementation of the QHA accommodates the possible change in lattice parameter/volume with temperature change. This addition is termed the *X-factor* in the vibrational Helmholtz energy, where *X* represents the lattice parameter or the volume. The relation for the QHA from the vibrational Helmholtz energy (F^{vib}) is given as:

$$F^{vib}(X,T) = \frac{1}{2}\sum_{\vec{q},\upsilon}\hbar\omega\,(\vec{q},\upsilon,X) + k_B T \sum_{\vec{q},\upsilon} In\left[1 - exp\left(\frac{-\hbar\omega(\vec{q},\upsilon,X)}{k_B T}\right)\right] \quad (11)$$

Where q is the wave-vector, the vibrational frequency is ω(q), k_B is the Boltzmann constant, T is temperature, $\hbar$ is the reduced Planck's constant, and υ is the frequency.

We neglect the effect of pressure in this report. The parameters analyzed and reported include the Debye temperature Θ_D, specific heat capacity at constant volume C_υ and its relation to the Dulong-Petit law, the average mean velocity, and the Debye entropy. The Debye temperature provides information on the thermal properties of the material at ambient and high temperatures. Table 4 presents the sound velocities (shear, compressional, and bulk), the average sound velocity, and the Debye temperature. We calculated the Debye temperature using the average mean velocity of sound as:

$$\Theta_D = \frac{h}{K_B}\left[\frac{3n}{4\pi}\frac{N_A\rho}{M}\right]^{1/3}\nu_m \quad (12)$$

Where h is Planck's constant, K_B is Boltzmann's constant, n is the number of atoms per unit cell, N_A is Avogadro's number, ρ is density, and M is the molecular weight. ν_m is the sound velocity at zero pressure. ν_m can be calculated using the longitudinal (V_l) and transverse (V_t) sound velocities obtained from the shear and bulk modulus using the Navier's equation [34] as

$$V_m = \left[\frac{1}{3}\left(\frac{2}{V_l^3} + \frac{1}{V_t^3}\right)\right]^{-1/3} \quad (13)$$

We present Navier's Equation for obtaining the sound velocities in Equations (17 & 18) and present results obtained from the calculations in Table 3.

$$V_l = \left[\left(B + \frac{4}{3}G\right)\frac{1}{\rho}\right]^{1/2} \quad (14)$$

$$V_t = \sqrt{\frac{G}{\rho}} \quad (15)$$

ρ is the density of the alloy, and other parameters retain their afore defined meanings. The alloy has an average sound velocity of 3421.230 m/s and a Debye temperature of 408.375 K. The result for Θ_D is consistent with the expectation that the main group element's atomic size has an inverse relationship with Θ_D. At 0 GPa and constant volume, the compound does not obey the Dulong Petit law, as evidenced in the specific heat capacity (Figure 4a). The Dulong-Petit limit is achieved at a temperature of about 680 K and C_υ of 73.5 $J\,mol^{-1}K^{-1}$ in agreement with Einstein's

contribution to the specific heat theory at high temperature. The Debye temperature and heat capacity behaviour with the Dulong-Petit law is consistent with other half Heusler compounds with similar atomic mass units [Osafile & Azi, 2020; Osafile & Umukoro, 2020; Musari et al., 2020; Adetunji et al., 2019]. We present the entropy change to temperature in Fig 4b. As expected, there is a rapid and continuous change in the compounds' entropy as temperature increases.

Table 4. *Results for the Voigt-Reuss-Hill average compressional, bulk and shear sound velocities (V_P, V_B, V_G) in m/s, the average Debye sound velocity υ_m in m/s, and the Debye temperature Θ_D in K of FeVAs and NiVGa alloys using QHA.*

compound	V_P	V_B	V_G	υ_m	Θ_D
RhVSi	6125.266	4987.175	3079.809	3421.230	408.375

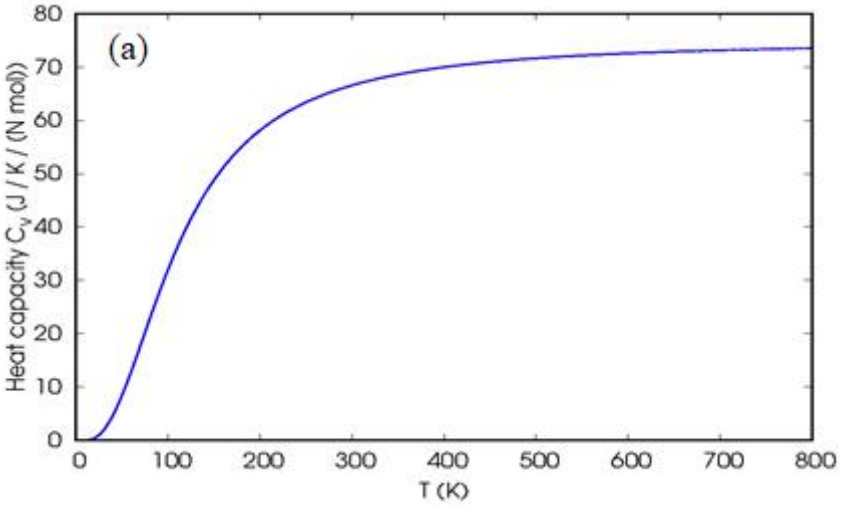

Figure 4a. *Specific heat capacity C_v of RhVSi hH alloy.*

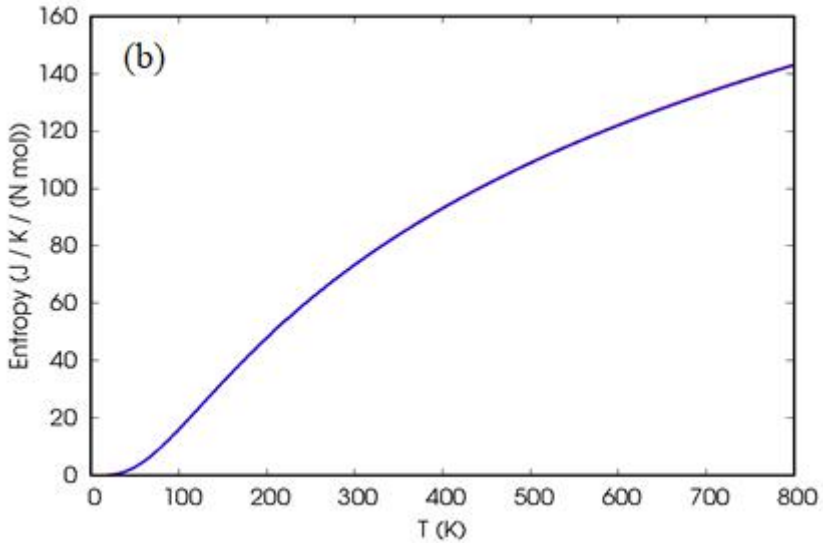

Figure 4b. *Entropy of RhVSi hH alloy with temperature change.*

3.4. Dynamical Stability

Lattice vibrations affect the phase stability of crystalline compounds. We have computed the phonon properties of the alloys using the thermo-pw as implemented in QE. We present the phonon dispersion curves along Γ→X→K→Γ→L→W→X symmetry directions here using a $4 \times 4 \times 4$ cubic supercell. However, up to now,

there have no experimental/other theoretical works exploring the lattice dynamics of the compound under zero pressure to compare with results obtained in this work.

The alloy investigated has three atoms in the unit cell; hence, the phonon dispersion spectra presented in Figure 5a displays six (6) optical modes and three (3) acoustic modes with non-negative frequencies. The phonon frequency corresponding to the dispersion is presented in Figure 5b. The absence of soft frequencies further ascertains that the compounds are both dynamically stable. The optical modes have a frequency range between 220 cm^{-1} and 330 cm^{-1} for the alloy, the exhibits the highest frequency band is observed between Γ and X. We observe a frequency gap in the interface between the optical modes and the acoustic modes across all bands of the first Brillouin zone. There is a dispersion at Γ in the optical mode, and this gives rise to one longitudinal optical (LO) phonon and two transverse optical (TO), we also observe a phonon splitting at L (~240 cm^{-1}). LO-TO splitting is the removal of degeneracy between the LO and TO phonons at the Brillouin zone centre. The LO-TO splitting is an essential parameter that aids in evaluating the strength of ionicity in bonding a material. The highest band in the optical mode is at X. In the acoustic mode, the dispersion at Γ produces one longitudinal acoustic (LA) phonon and two transverse acoustic (TA) phonons at X (120 cm^{-1}) and L (105 cm^{-1}).

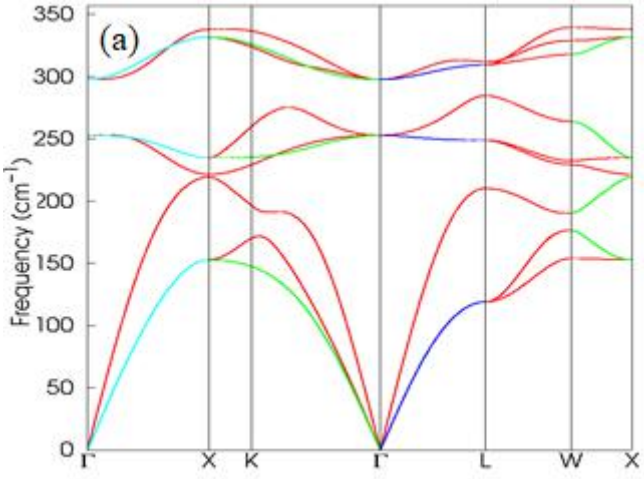

Figure 5a. *Phonon dispersion of RhVSi hH alloy.*

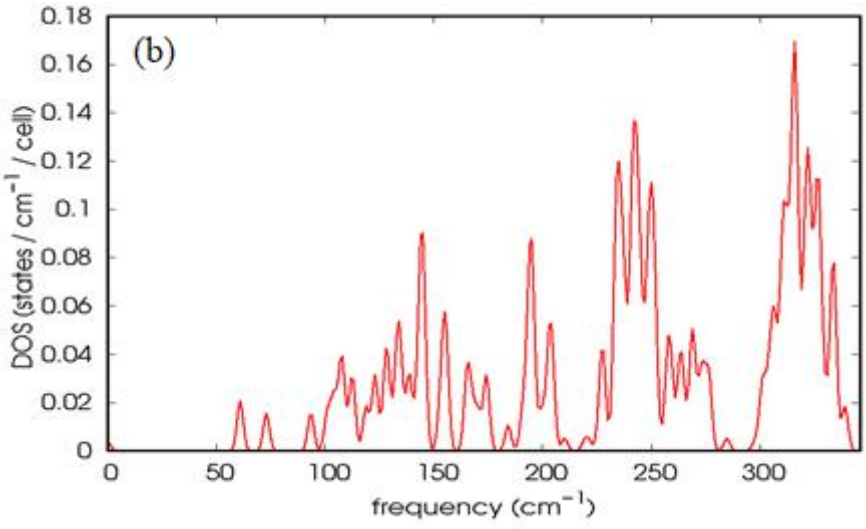

Figure 5b. *Density of states frequency of RhVSi hH alloy.*

4. Conclusions

We have investigated RhVSi 18-valence electron half Heusler alloy's structural and electronic stability from first principles using the density functional theory implemented in the quantum espresso computational code. The alloy obeys the Slater-Pauling rule for 18-valence electrons; as expected, it is a semiconductor. The alloy displays an indirect narrow-bandgap in a stable face-centred cubic structure. The result we obtained for the lattice constant compare well with the result reported in literature. We also investigated for the first time the elastic, mechanical, thermodynamic, and phonon properties of RhVSi alloy using the linear response quasi-harmonic approximation method and the density functional perturbation theory as implemented in thermo-pw code. Reports show that RhVSi alloy is ductile and super hard. The alloy obeys the Dulong-Petit limit at a temperature of 680 K and C_{υ} of 73.5 $J\ mol^{-1}K^{-1}$ with a Debye temperature of 408.375 K. The Debye temperature shows that the compound is hard and possesses a large wave velocity (3421.230 m/s) and will have high thermal conductivity. From the phonon calculations, and there are no negative frequencies. The thermodynamic and phonon test results predict RhVSi to be a stable semiconductor that can be simulated experimentally. We hope that the present work will spurn the interest of experimentalists to fabricate the alloy.

Conflicts of Interest

The author declares that there is no conflict of interest regarding the publication of this article.

Funding

This research received no specific grant from any funding agency in the public, commercial or not-for-profit sectors.

References

[1] Heusler, F. Über magnetische manganlegierungen. *Verhandlungen der Deutschen Physikalischen Gesellschaft,* 1903, 5, 219.

[2] De Groot, R. A.; Mueller, F.M.; Van Engen, P.G.; Buschow, K.H.J. New class of materials: half-metallic ferromagnets. *Phys. Rev. Lett,* 1983, 50(25), 2024-2027.

[3] Bainsla, L.; Suresh, K.G.; Nigam, A.K.; Manivel Raja, M.; Varaprasad, B.C.S.; Takahashi, Y. K.; Hono, K. High spin polarization in CoFeMnGe equiatomic quaternary Heusler alloy. *Journ. of App. Phy.* 2014, 116(20), 203902-203906.

[4] Bainsla, L.; Suresh, K.G. Equiatomic quaternary Heusler alloys: A material perspective for spintronic applications. *Applied Physics Reviews,* 2016, 3(3), 031101-21.

[5] Liu, H.X.; Kawami, T.; Moges, K.; Uemura, T.; Yamamoto, M.; Shi, F.; Voyles, P.M. Influence of film composition in quaternary Heusler alloy Co_2(Mn,Fe) Si thin films on tunnelling magnetoresistance of Co_2(Mn,Fe) Si/MgO-based magnetic tunnel junctions. *Journ. of Phy. D: App. Phy.* 2015, 48(16), 164001-9.

[6] Chen, S.; Ren, Z. Recent progress of half-Heusler for moderate temperature thermoelectric applications. *Materials today,* 2013, 16(10), 387-395.

[7] Amudhavalli, A.; Rajeswarapalanichamy, R.; Iyakutti, K.; Kushwaha, A. K. First principles study of structural and optoelectronic properties of Li based half Heusler alloys. *Comp. Cond. Mat.* 2018, 14, 55-66.

[8] Osafile, O.E.; Azi, J.O. Structural, electronic, elastic and mechanical properties of novel ZrMnAs half Heusler alloy from first principles. *Physica B: Condensed Matter,* 2019, 571, 41-49.

[9] Xie, H.; Wang, H.; Pei, Y.; Fu, C.; Liu, X.; Snyder, G. J. et al.. Beneficial contribution of alloy disorder to electron and phonon transport in half-heusler thermoelectric materials. *Adv. Funct. Mat.* 2013, 23(41), 5123-5130.

[10] Rogl, G.; Grytsiv, A.; Gürth, M.; Tavassoli, A.; Ebner, C.; Wünschek, A. et al. Mechanical properties of half-Heusler alloys. *Acta Materialia,* 2016, 107, 178-195.

[11] Singh, S.; Bhat, T. M.; Gupta, D.C. Effect of High Pressure and Temperature on Magneto-Electronic, Thermodynamic, and Transport Properties of Antiferromagnetic HoPdX (X= As, Ge) Alloys. *Journal of Superconductivity and Novel Magnetism,* 2019, 32(7), 2051-2065.

[12] Surucu, G.; Candan, A.; Erkisi, A.; Gencer, A.; Güllü, H.H. First principles study on the structural, electronic, mechanical and lattice dynamical properties of XRhSb (X= Ti and Zr) paramagnet half-Heusler antimonides. *Materials Research Express,* 2019, 6(10), 106315-106329.

[13] Roy, A.; Bennett, J.W.; Rabe, K.M.; Vanderbilt, D. Half-Heusler semiconductors as piezoelectrics. *Physical review letters,* 2012, 109(3), 037602-037607.

[14] Casper, F.; Graf, T.; Chadov, S.; Balke, B.; Felser, C. Half-Heusler compounds: novel materials for energy and spintronic applications. *Semicond. Sci. and Technol.* 2012, 27(6), 063001-063008.

[15] Giannozzi, P.; Baroni, S.; Bonini, N.; Calandra, M.; Car, R.; Cavazzoni, C. et al. QUANTUM ESPRESSO: a modular and open-source software project for quantum simulations of materials. *Journal of physics: Condensed matter,* 2009, 21(39), 395502.

[16] Kresse, G.; Joubert, D. From ultrasoft pseudopotentials to the projector augmented-wave method. 1999. *Phys. Rev. B,* 1999, 59(3), 1758-1775.

[17] Burke, K.; Perdew, J.P.; Ernzerhof, M. Why semilocal functionals work: Accuracy of the on-top pair density and importance of system averaging. *The Journal of chemical physics,* 1998, 109(10), 3760-3771.

[18] Perdew, J.P.; Burke, K.; Ernzerhof, M. Generalized gradient approximation made simple. *Phy. Rev. lett,* 1996, 77(18), 3865-3868.

[19] Monkhorst, H.J.; Pack, J.D. Special points for Brillouin-zone integrations. *Phy. Rev. B,* 1976, 13(12), 5188-5192.

[20] Murnaghan, F.D. Finite deformations of an elastic solid. *American Journal of Mathematics,* 1937, 59(2), 235-260.

[21] Birch, F. Finite elastic strain of cubic crystals. *Physical review,* 1947, 71(11), 809-824.

[22] Murnaghan, F.D. The compressibility of media under extreme pressures. *Proceedings of the national academy of sciences of the United States of America,* 1944, 30(9), 244.

[23] Kokalj, A. XCrySDen-a new program for displaying crystalline structures and electron densities. *Journal of Molecular Graphics and Modelling,* 1999, 17(3-4), 176-179.

[24] Voigt, W. Lehrbuch der Kristallphysik (Textbook of crystal physics). BG Teubner, Leipzig und Berlin, 1928.

[25] Reuss, A. Calculation of the flow limit of solid solution based on the plasticity condition for single crystals. *ZAMM - Journal of Applied Mathematics and Mechanics / Zeitschrift für Angewandte Mathematik und Mechanik,* 1929, 9 (1), 49-58.

[26] Hill, R. The elastic behaviour of a crystalline aggregate. *Proceedings of the Physical Society. Section A,* 1952, 65(5), 349.

[27] Zhang, Y.; Xu, X. Machine learning modeling of lattice constants for half-Heusler alloys. *AIP Advances,* 2020, 10 (4), 045121-10.

[28] Born, M.; Huang, K. Dynamical theory of crystal lattices. Clarendon press, 1954.

[29] Harmening, T.; Eckert, H.; Pöttgen, R. Defects in half-Heusler type antimonides ScTSb (T= Ni, Pd, Pt). *Solid state sciences,* 2009, 11(4), 900-906.

[30] Frantsevich, I.N.; Voronov, F.F.; Bakuta, S.A. Elastic constants and elastic moduli of metals and non-metals(In Russian). *Kiev, Izdatel'stvo Naukova Dumka,* 1982, 288.

[31] Pugh, S.F. XCII. Relations between the elastic moduli and the plastic properties of polycrystalline pure metals. *The London, Edinburgh, and Dublin Philosophical Magazine and Journal of Science,* 1954, 45(367), 823-843.

[32] Tian, Y.; Xu, B.; Zhao, Z. Microscopic theory of hardness and design of novel superhard crystals. *International Journal of Refractory Metals and Hard Materials,* 2012, 33, 93-106.

[33] Hopcroft, M.A., Nix, W.D.; Kenny, T.W. What is the Young's Modulus of Silicon? *Journal of microelectromechanical systems,* 2010, 19(2), 229-238.

[34] Anderson, O.L. A simplified method for calculating the Debye temperature from elastic constants. *Journal of Physics and Chemistry of Solids,* 1963, 24(7), 909-917.

[35] Adetunji, B.I.; Adebambo, P.O.; Bamgbose, M.K.; Musari, A.A.; Adebayo, G.A. Predicting the elastic, phonon and thermodynamic properties of cubic HfNiX (X= Ge and Sn) Half Heulser alloys: a DFT study. *The Euro. Phys. Journal B,* 2019, 92(10), 1-7.

[36] Osafile, O.E.; Azi, J.O. First principles prediction of structural, mechanical and thermodynamic stability in new 18-valence electron XVZ (X= Fe, Ni, Z= Ga, As) half-Heusler semiconductors. *Semiconductor Science and Technology,* 2020, 35(10), 105005.

[37] Musari, A.A.; Adetunji, B.I.; Adebambo, P.O.; Adebayo, G.A. Lattice dynamics and thermodynamic investigation of MNiSn (M= Hf, Ti and Zr) Half-Heusler

compounds: Density functional theory approach. *Materials Today Communications,* 2020, 22, 100671.

[38] Osafile, O.E.; Umukoro, J.O. Quasi-harmonic approximation of lattice dynamics and thermodynamic properties of half Heusler ScXSb (x= Ni, Pd, Pt) from first principles. *Journal of Physics: Condensed Matter,* 2020, 32(47), 475504.